*Exploration Geophysics (2006) **37**, 93-101*
*Butsuri-Tansa (Vol. 59, No. 1)*
*Mulli-Tamsa (Vol. 9, No. 1)*

# Joint inversion of receiver function and surface-wave phase velocity for estimation of shear-wave velocity of sedimentary layers

**Takeshi Kurose** [1] **Hiroaki Yamanaka**

**Key Words**: receiver function, surface wave, phase velocity, microtremor array survey, joint inversion, sedimentary layer, genetic algorithms

## ABSTRACT

In this study, we propose a joint inversion method, using genetic algorithms, to determine the shear-wave velocity structure of deep sedimentary layers from receiver functions and surface-wave phase velocity. Numerical experiments with synthetic data indicate that the proposed method can avoid the trade-off between shear-wave velocity and thickness that arises when inverting the receiver function only, and the uncertainty in deep structure from surface-wave phase velocity inversion alone. We apply the method to receiver functions obtained from earthquake records with epicentral distances of about 100 km, and Rayleigh-wave phase velocities obtained from a microtremor array survey in the Kanto Plain, Japan. The estimated subsurface structure is in good agreement with the previous results of seismic refraction surveys and deep borehole data.

## INTRODUCTION

The shear-wave velocity structure in sedimentary layers, down to the basement with an S-wave velocity of about 3 km/s, is essential information for precisely estimating or predicting strong-motion characteristics during earthquakes. To explore the shear-wave velocity structure of deep sedimentary layers, inversion of surface-wave phase velocities obtained from a microtremor array survey was developed (Horike, 1985; Okada, 2003). The applicability of the microtremor array method has been confirmed by many actual surveys performed on large-scale sedimentary basins in Japan (e.g., Kagawa et al., 1998; Yamanaka and Yamada, 2002), and it has been established as a convenient and low-cost method of providing an S-wave profile of deep sediments for engineers in earthquake engineering.

The microtremor array method utilises dispersion of surface waves, commonly Rayleigh waves, contained in observed microtremor array data. In order to determine accurately a profile from near-surface to basement by this technique alone, microtremors must be observed over a broad frequency range, and phase velocity must be estimated precisely over this range, because deeper structure influences surface-wave dispersion at longer periods. However, the period range of observed microtremor data is generally limited because of the inherent small amplitude of long-period microtremors, and the limited array aperture. For example, Yamanaka et al. (1995) pointed out that the inversion of Rayleigh-wave phase velocity up to a period of 5 seconds only, in a microtremor array survey performed in Tokyo, Japan, resulted in lower resolution in deep structure. They, however, inverted Rayleigh-wave phase velocity data simultaneously with Love-wave phase velocities up to a period of 10 seconds, obtained from earthquake records, to improve the resolution in the deep structure.

A receiver-function method was originally developed to explore the shear-wave velocity structure of the crust and mantle, using mainly broadband earthquake records (Langston, 1979). The method uses seismic phases generated from P-S conversions and multiple reflections at velocity discontinuities. Inversion of the receiver function (Owens et al., 1984) is an established method that many researchers use to explore the crust and mantle (e.g., Darbyshire et al., 2000; Last et al., 1997; Priestley et al., 1988). Recently, the receiver function has also been attracting attention in earthquake engineering, as a method of estimating basement depth using the arrival time difference between direct P and P-S converted waves (Kobayashi et al., 1998). However, their application of the method uses only P-S converted phases from the sediment/basement boundary, and does not use the whole receiver function. Even if the P-S conversion generated at the top of the basement is accurately identified, the arrival time difference between direct P waves and the P-S converted waves cannot be directly converted to basement depth without a priori information on the subsurface structure at the target site. It should also be noted that the inversion method proposed by Owens et al. (1984) is based on a damped least-squares technique, which may sometimes suffer from numerical instability, and give inversion results that depend on the choice of initial model. In order to avoid these problems, global optimisation algorithms, such as genetic algorithms and simulated annealing, were applied to inversion of the receiver function by Shibutani et al. (1996) and Zhao et al. (1996), for example. It is well known that there must be a trade-off between shear-wave velocity and thickness in inversion of receiver functions (Ammon et al., 1990). In order to avoid this problem, Julia et al. (2000) performed a joint inversion of the receiver function with surface-wave group velocities, in crust and mantle studies. It is widely considered that inversion of different kinds of observation simultaneously is an effective method of avoiding the common problems of correlation between parameters or non-uniqueness of inversion results, arising from inverting only one type of observed data (e.g., Vozoff and Jupp, 1974).

In this study, we propose a joint inversion method, using genetic algorithms, to estimate the shear-wave velocity structure of deep sedimentary layers from receiver function and surface-wave phase velocity data. We discuss the applicability of the method, trade-off between parameters, and the uniqueness of the inversion result, using numerical experiment and analysis of actual observed data.

*Interdisciplinary Graduate School of Science and Engineering,*
*Tokyo Institute of Technology*
*4259, Nagatsuta-cho, Midori-ku, Yokohama, Kanagawa, 226-8502, Japan*
*Tel: +81-45-924-5513*
*Fax: +81-45-924-5514*
*Email: yamanaka@depe.titech.ac.jp*

*CRC Solutions Corp.*
*2-7-5, Minamisuna, Koto-ku, Tokyo, 136-8581, Japan*

*Manuscript received 1 August, 2005.*
*Revised manuscript received 7 November, 2005.*

 

## JOINT INVERSION METHOD

Here we present our joint inversion method for receiver function and Rayleigh-wave phase velocity data obtained at a common site. We use a genetic algorithm to infer a 1D S-wave velocity profile of the subsurface layers that can fit the two kinds of data.

It often happens in exploration of sedimentary layers that there is little a priori information about the subsurface structure at a target site, which makes it difficult to set an appropriate initial model for a least-squares inversion method. Therefore, we have applied a genetic algorithm (GA) to the joint inversion. Recently, GAs have been applied to many inverse problems in seismology and geophysical exploration because of their applicability to global optimisation problems (e.g., Sambridge and Drijkoningen, 1992; Sambridge and Gallagher, 1993; Yamanaka and Ishida, 1996; Zhou et al., 1995). The GA that we implemented here was similar to that of Yamanaka and Ishida (1996), which adopted a binary coding and introduced an elite selection and dynamic mutation, except for the definition of misfit, which is to be minimised in the inversion.

The dimensions and number of the receiver function and phase velocity data are different from each other. So the data must be reduced to dimensionless form in order to invert them simultaneously. Hence, the objective function (goodness of fit) for the receiver function $\phi_{RF}$, and that for the phase velocity $\phi_{ph}$, are defined as the sum of squared differences between the observations and calculated values, normalised by the standard deviation and divided by the number of data as shown in equation (1).

$$\varphi_{RF} = \left(\frac{1}{N_{RF}}\right)\sum_i \left[\frac{R_{obs}(t_i) - R_{cal}(t_i)}{\sigma_{RF}(t_i)}\right]^2 \qquad (1)$$

$$\varphi_{ph} = \left(\frac{1}{N_{ph}}\right)\sum_j \left[\frac{C_{obs}(T_j) - C_{cal}(T_j)}{\sigma_{ph}(T_j)}\right]^2 .$$

Here, $N_{RF}$ and $N_{ph}$ are the number of data and $\sigma_{RF}(t_i)$ and $\sigma_{ph}(T_j)$ are the standard deviations of the observed receiver function $R_{obs}(t_i)$ at time $t_i$ and the observed phase velocity $C_{obs}(T_j)$ at period $T_j$, respectively. The objective function $\phi$ to be minimised in the joint inversion is defined as the weighted sum of $\phi_{RF}$ and $\phi_{ph}$:

$$\varphi = p\varphi_{ph} + (1-p)\varphi_{RF} \cdot \qquad (2)$$

Here, $p$ is a parameter ranging from 0 to 1, representing the weight placed on the phase velocity data. If $p$ is 0 or 1, equation (2) represents individual inversion of either receiver function or phase velocity data. The factor $p$ corresponds to the "influence parameter" used by Julia et al. (2000).

In the joint inversion, parameters of the subsurface structure at a target site are determined so that the misfit defined by equation (2) will be minimised for a value of $p$ given in advance. Theoretical receiver function and Rayleigh-wave phase velocity values are calculated using P- and S-wave velocities, thickness, and density of each layer in a flat-layered model. However, S-wave velocity and thickness are the most influential quantities (e.g., Horike, 1985). Therefore, S-wave velocity and thickness of each layer are parameterised in the inversion. P-wave velocity is calculated from S-wave velocity using an empirical relationship established from velocity data in deep sediments in Japan (Kitsunezaki et al., 1990). Densities are fixed at constant values. The theoretical receiver function, $R_{cal}(t_i)$, and the theoretical phase velocity, $C_{cal}(T_j)$, in equation (1) are calculated by the methods of Haskell (1962) and Haskell (1960), respectively.

In the GA implementation, the population size and rates of crossover and mutation are set to be 30, 0.7, and 0.01, respectively. Each parameter was coded into an 8-bit binary string. Selection was performed according to a roulette rule. The inversion result was evaluated after 10 repetitions of a 100-generation calculation with different seeds of random number generator. Further details of the parameters in the GA can be seen in Yamanaka and Ishida (1996).

## NUMERICAL EXPERIMENT

A subsurface structural model used in the numerical experiment is shown in Table 1. This is a typical model of deep sedimentary layers down to basement, where S-wave velocity is 3.0 km/s, in the Kanto Basin, Japan (Yamanaka and Yamada, 2002). Synthetic receiver function values and fundamental-mode Rayleigh-wave phase velocities for the model were calculated, and contaminated with two sets of random noise, uncorrelated with each other, as shown in Figures 1(a) and 1(b). These synthetic data were used in the numerical test. The noise added to the receiver function lies in the range of ±0.2 from the synthetics, while we added 10% noise to the phase velocity. As explained earlier, phase velocity data are not always perfectly observed in an actual survey. Therefore, we used only the phase velocities at periods shorter than 4.5 s in the test, as shown in Figure 1(a). In the calculation of the

| | True Model | | | | Search Area | |
|---|---|---|---|---|---|---|
| Layer | Vp (km/s) | Vs (km/s) | H (km) | ρ (t/m³) | Vs (km/s) | H (km) |
| 1 | 1.96 | 0.6 | 0.3 | 1.8 | 0.3–0.8 | 0.1–1.0 |
| 2 | 2.40 | 1.0 | 1.0 | 2.0 | 0.8–1.8 | 0.1–1.5 |
| 3 | 3.29 | 1.8 | 0.7 | 2.3 | 1.5–2.0 | 0.1–1.5 |
| 4 | 4.62 | 3.0 | ∞ | 2.5 | 3.0 | ∞ |

**Table 1. Subsurface structural model and search limits for a numerical experiment in inversion. Vp is assumed from the relation between Vp and Vs found by Kitsunezaki et al. (1990).**

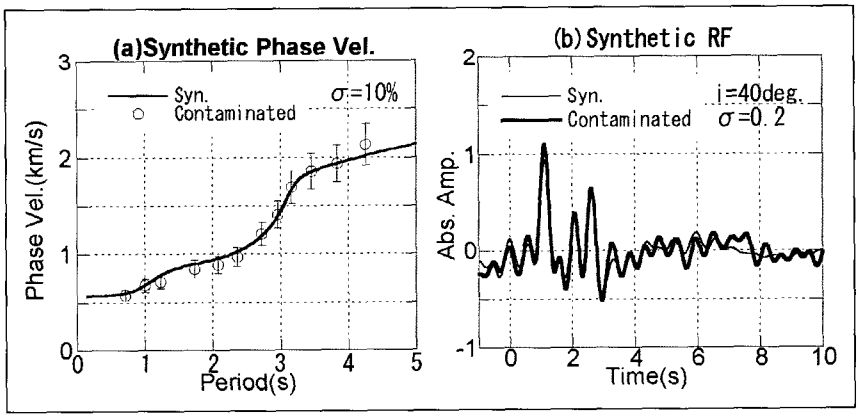


**Fig. 1. Comparison of fundamental-mode Rayleigh-wave phase velocity and receiver function data for the model in Table 1 with those used in numerical experiments. (a) Phase velocity for the true model (solid line) and test data (circles). (b) Receiver functions for true model (thin line) and test data contaminated with random noise (thick line).**

synthetic receiver function, the incident angle of the P-wave at the top of basement was set to be 40°, and a band-pass filter in the period range from 0.5 s to 5.0 s was applied. We also assumed a frequency-independent Q-value to be defined by 1/15 of P- or S-wave velocity in m/s. Standard deviation of the receiver function, $\sigma_{RF}$ in equation (1), was set to be 0.2 uniformly, while that of the phase velocity, $\sigma_{ph}$ , was set to be 10% of the noisy synthetic value. Test calculations were performed with the values of $p$ in equation (2) from 0.1 to 0.9 with an interval of 0.2. The cases of $p = 0$ and $p = 1$ were also tested for comparison. Search limits for S-wave velocities and thicknesses of each layer are also shown in Table 1.

S-wave profiles obtained from the inversions for all the values of $p$, from 0 to 1, are shown in Figure 2, together with the true model. The final models were determined by averaging parameters from acceptable solutions, as explained later. The comparison of the test data and the synthetics obtained from the inversion result with $p = 0.5$ is also shown in Figures 3(a) and 3(b). The results of the joint inversion (with $p$ from 0.1 to 0.9), are in better agreement with the true model than the result of individual inversion of either the phase velocity only ($p = 1$) or receiver function only ($p = 0$). The difference in basement depth between the true model and the individual inversion of phase velocity data is quite large. The model from inversion of the receiver function data also differs from the true model in the S-wave velocity of the first layer. Because each individual inversion attempts to find an optimum model to satisfy the contaminated data without any other constraints, the results of the individual inversions are quite different from the true model. On the other hand, the models obtained from joint inversions, at all values of $p$, are not widely different from the true model. This indicates that the joint inversion tries to find the optimum model referring to the two datasets. The remarkable differences between the model for $p = 1$ and the model for $p = 0.9$ should be also noted (Figure 2). This shows that even the slightest contribution from the receiver function data in the inversion performs a constraining role in the resultant model. Consequently, the joint inversion of receiver function and surface-wave phase velocity data can reduce the effects of noise contained in each dataset.

Next, we evaluate uniqueness of the inversion results by using the concept of "acceptable solutions" introduced by Lomax and Snieder (1994). The outline of the concept is described in the following way. In general, the objective function (misfit) surface in nonlinear inverse problems is so complex that many local minima with slightly larger misfits than that of the global minimum may exist. Many models found by the GA inversion are considered to be located near the global minimum. However, some of them may be trapped in local minima, because of the complexity of the misfit surface and premature convergence in the GA. Therefore, the models with misfits lower than a misfit threshold are selected as "acceptable solutions", as shown in Figure 4. If the misfit surface has two local minima with misfits similar to the global minimum as in Figure 4(a), the parameters of the acceptable solutions are distributed in three separate areas in parameter space. However, where there is no local minimum with a misfit comparable to the global minimum, as shown in Figure 4(b), the parameters of the acceptable solutions are distributed in only one area, ideally near one single point. Therefore, the uniqueness of the inversion result can be approximately evaluated from the parameter distributions of the acceptable solutions.

The parameter distributions of the acceptable solutions obtained from the test result are shown in Figure 5 for each value of $p$. The search limits for the parameters of each layer are also depicted in the figure. The threshold of the misfit for determining the acceptable solutions, $\phi_{acceptable}$, is calculated from the following equation.

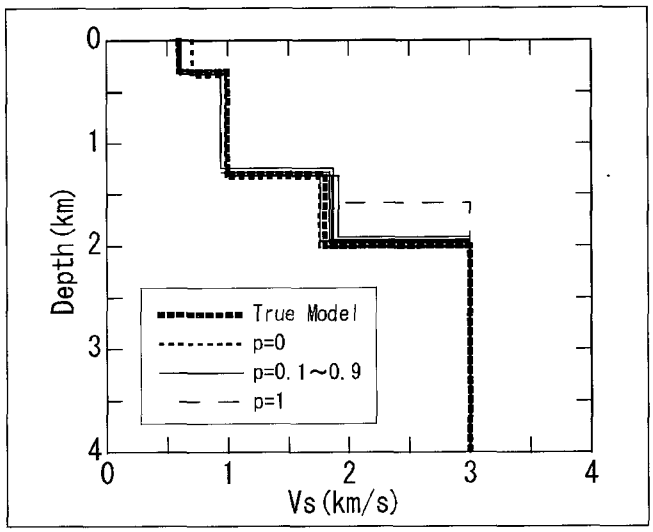


**Fig. 2. Comparison of test data for the numerical experiment with synthetic data for the model from joint inversion with $p = 0.5$. a) Fundamental-mode Rayleigh-wave phase velocity; b) Receiver function.**

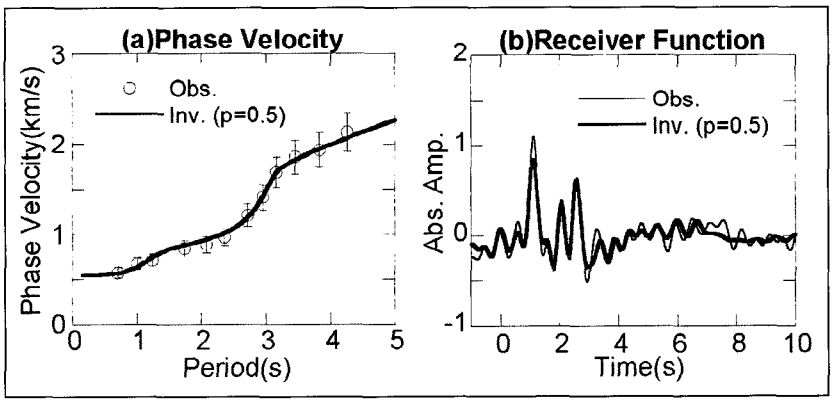


**Fig. 3. Comparison of true model and inversion results with different values of $p$ in the numerical test.**

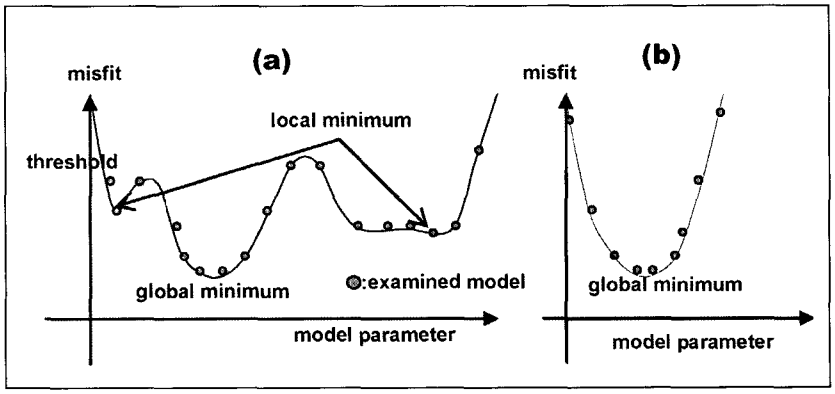


**Fig. 4. Schematic diagram of misfit surface and acceptable solutions. a) A case where there are many local minima with misfits nearly equal to the global minimum. b) A case where there is no local minimum nearly equal to the global minimum.**

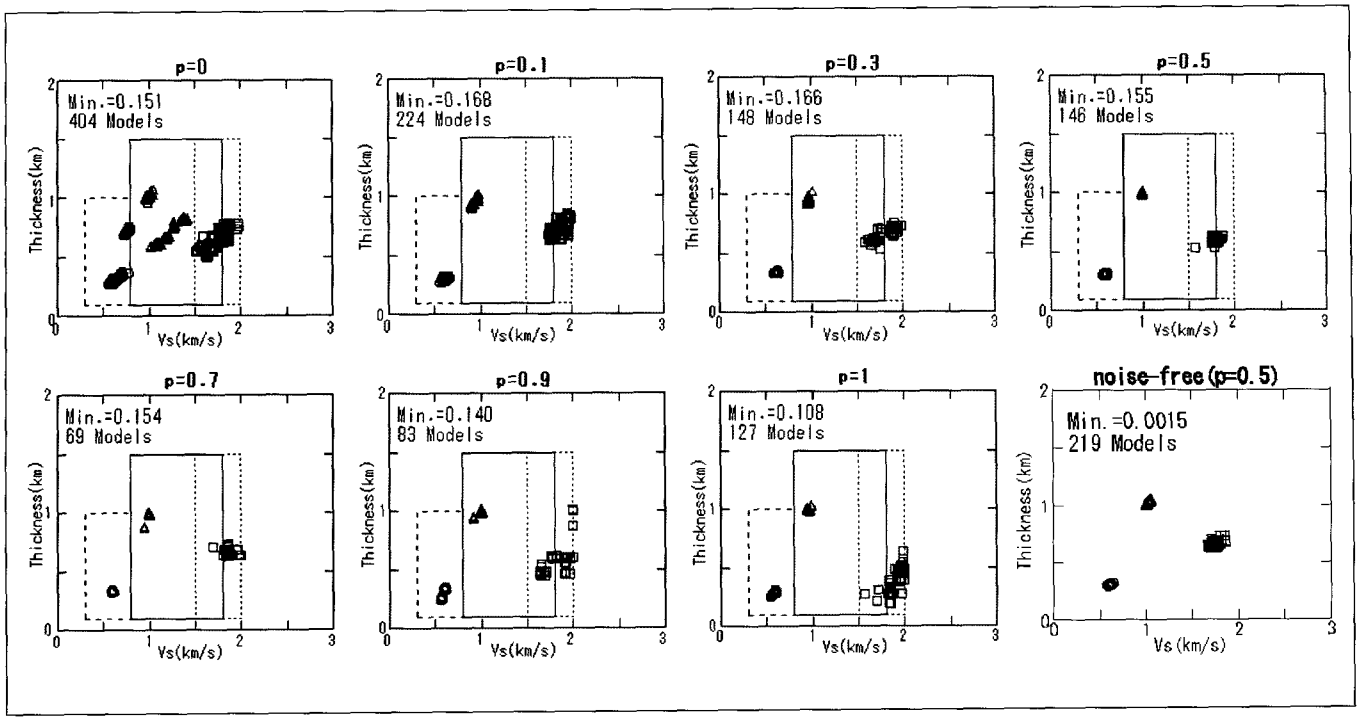


**Fig. 5. Parameter distributions for acceptable solutions for each value of $p$. The threshold was set to be the minimum misfit plus 0.05. Circles, triangles, and squares indicate the parameters of the first, second, and third layers, respectively. Rectangular areas shown by solid and broken lines indicate search limits for parameters of each layer. Results from joint inversion of noise-free test data is also shown in the lower-left figure.**

$$\varphi_{\text{acceptable}} = \varphi_{\text{min}} + \varepsilon \quad . \tag{3}$$

Here $\phi_{\text{min}}$ is the minimum misfit found by all the inversions, and $\varepsilon$ was set to be 0.05. This value is determined by a trial-and-error procedure. The values of the minimum misfit and the numbers of acceptable solutions can be seen in Figure 5. The parameters of the acceptable solutions are averaged to obtain a final model.

The case of $p = 0$ (the individual inversion of the receiver function) shows that the parameters of acceptable solutions for the first and second layers are distributed in two separated areas. This means that there are two minima, at least, with nearly equal misfits on the misfit surface. The parameters for the third layer are distributed in one cluster, but its area is comparatively large suggesting lesser resolution in the third layer. It should be also noted that many acceptable solutions seem to be distributed around an inclined line, indicating a constant ratio between thickness and S-wave velocity. Since the information contained in the receiver function is the travel times of each P-S converted wave, and multiples, relative to the travel time of the direct P-wave, different models might produce quite similar receiver functions if the relative travel times obtained from those models are almost equal. Therefore, the linear relationship of the parameter distribution can be attributed to the trade-off between S-wave velocity and thickness in a receiver function (Ammon et al., 1990). In the case of $p = 1$ (the individual inversion of the phase velocity) the parameters of the first and second layers are distributed around one single point, suggesting that unique optimum values were determined in the inversion. However, the parameter distribution for the third layer shows a deterioration of the resolution, because of the limited period range of the phase velocities used in the test. The cases for $p = 0.1$ and $p = 0.3$ indicate no trade-off relationships, and the parameters of the acceptable solutions are distributed over a much smaller area than is the case for $p = 0$. This means that the misfit surface near the global minimum becomes much simpler than when modelling only the receiver function, if even a small influence of the phase velocity data is introduced. The cases for $p = 0.7$ and 0.9 indicate rather high resolution for the parameters of the first and second layers, but uncertainty for the third layer as in the case of $p = 1$. In the case of $p = 0.5$, the parameters for all layers are distributed in the smallest areas indicating that there are no local minima with a nearly equal misfit to the global minimum. Therefore, the choice of $p = 0.5$ can reduce the effects of the correlation between parameters, and the uncertainty in deep structure, which leads to a unique optimum model.

The parameter distributions of the acceptable solutions from the joint inversion of noise-free synthetic receiver function and phase velocity data in Figure 1 are also shown in Figure 5 with $p = 0.5$. The misfit is significant smaller than those from the inversions of the test data with noise, suggesting the existence of a narrow trough at the global minimum in the misfit surface. Most of the parameters are located near the true value. It is noted that the parameter distributions for the acceptable solutions from the inversions with and without noise are similar. This suggests that the method is definitely applicable to noisy data.

## APPLICATION OF JOINT INVERSION TO ACTUAL DATA

We applied the joint inversion method to receiver function and phase velocity data observed in the Tokyo Metropolis, Japan. Recently, many seismological stations have been installed in the area. We used earthquake records observed at the Tokyo Observatory of the Japan Meteorological Agency for calculating the receiver function, because it is one of the older stations, and many earthquake records have been accumulated through long-term observation. Rayleigh-wave phase velocity data were obtained from a microtremor array survey performed in downtown Tokyo (Yamanaka et al., 1995). Locations of the two sites are shown in Figure 6(a). The epicentres of earthquakes used in the calculation of the receiver function are shown in Table 2 and Figure 6(b). Although the two sites are separated by a distance of about 5 km, this area is topographically flat and it is assumed that the subsurface structure does not change, so that it can be described as a simple flat-layered model (Koketsu, 1995). Therefore, it is

considered to be reasonable to apply the joint inversion method to the datasets described above.

### Observed Phase Velocity

Yamanaka et al. (1995) performed a microtremor array survey in downtown Tokyo, at the KOTO site shown in Figure 6(a). They estimated Rayleigh-wave phase velocity at periods from 0.8 to 4.3 s, as shown in Figure 7. Since their phase velocity is limited in period range, they pointed out the difficulty of deducing an accurate S-wave velocity for the deeper sediments. They also estimated a basement depth from a joint inversion of the Rayleigh-wave phase velocity described above and Love-wave phase velocity data, with periods of about 5 to 10 s, obtained from earthquake records observed near the array site during an earthquake. The resulting S-wave velocity profile was in good agreement with seismic refraction surveys (Koketsu, 1995) and deep borehole data (Suzuki, 1999).

### Observed Receiver Functions

The water-level method of calculating receiver functions from earthquake records was used in this study (Langston, 1979). The outline of the method is explained in the following paragraphs.

Observed spectra of radial and vertical components of an incident P-wave can be described as follows:

$$D_{rad}(\omega) = I(\omega)S(\omega)E_{rad}(\omega)$$
$$D_{ver}(\omega) = I(\omega)S(\omega)E_{ver}(\omega) \quad (4)$$

Here $I(\omega)$ is the instrument response, $S(\omega)$ is the source spectrum, and $E_{rad}(\omega)$ and $E_{ver}(\omega)$ are the radial and vertical response of the subsurface structure of the target site. The division of $D_{rad}(\omega)$ by $D_{ver}(\omega)$ will remove $I(\omega)$ and $S(\omega)$, resulting in the extraction of the terms of $E_{rad}(\omega)$ and $E_{ver}(\omega)$. Langston (1979) formulated this as follows.

$$R_{rad}(\omega) = D_{rad}(\omega)D^{*}_{ver}(\omega)G(\omega)/\psi(\omega)$$
$$\psi(\omega) = \max\left\{D_{ver}(\omega)D^{*}_{ver}(\omega), c\max\left\{D_{ver}(\omega)D^{*}_{ver}(\omega)\right\}\right\} \quad (5)$$

Here, $c$, which is called "water-level", is introduced in order to avoid instability caused by a very small denominator. The asterisk indicates the complex conjugate and $G(\omega)$ is a filter. The inverse Fourier transform of $R_{rad}(\omega)$ gives the receiver function, $R_{rad}(t)$. In this study, the water-level was fixed to be 0.01.

Earthquake data used in the calculation of receiver functions were obtained during earthquakes that occurred in the east, off Izu Peninsula, as shown in Figure 6(b) and Table 2. The Langston method of estimating receiver functions was applied to the first 10 s from the onset of the P-wave in these records. The resultant receiver functions are shown in Figure 8. A band-pass filter, with a period range from 0.5 to 5.0 s, was applied during the calculations. Distinct phases can be seen at 1.7 s and 3.9 s from the P-wave onset in the observed receiver functions. It is considered that the first phase represents a P-S converted wave generated at the sediment/basement interface. These receiver functions were stacked to form the average receiver function as shown in Figure 9. This was used in the subsequent joint inversion.

| No. | Date (dd/mm/yyyy) | Time | Lat. (deg) | Lon. (deg) | Depth (km) | M | Δ (km) | θ (deg) |
|---|---|---|---|---|---|---|---|---|
| 1 | 01/08/1988 | 1:10 | 34.93 | 139.25 | 23 | 4.2 | 96 | 209 |
| 2 | 05/07/1989 | 2:28 | 34.91 | 139.26 | 48 | 4.3 | 98 | 207 |
| 3 | 07/07/1989 | 0:01 | 34.98 | 139.16 | 21 | 5.3 | 95 | 215 |
| 4 | 09/07/1989 | 11:09 | 34.96 | 139.13 | 24 | 5.5 | 99 | 215 |
| 5 | 22/01/1995 | 17:01 | 34.93 | 139.35 | 28 | 4.0 | 92 | 203 |

**Table 2. List of earthquakes used in the calculation of receiver functions. $\Delta$ is an epicentral distance and $\theta$ is a backazimuth.**

### Joint Inversion

The angle of incidence of the P-wave at the sediment/basement interface was estimated from the P-wave velocity structure of the crust and mantle in this area, shown in Figure 10.

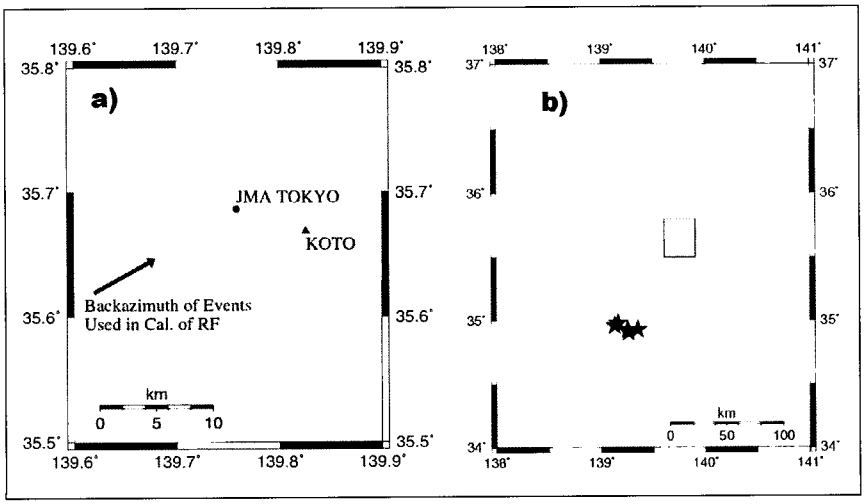


**Fig. 6. Map for stations and epicentres. a) Locations of Tokyo Observatory of the Japan Meteorological Agency (JMA) and the microtremor array site, KOTO, by Yamanaka et al. (1995). The map also shows backazimuth directions of earthquakes used in calculation of receiver function. b) Locations of epicentres of earthquakes used in the calculation of receiver functions. The rectangle corresponds to the area shown in the left figure.**

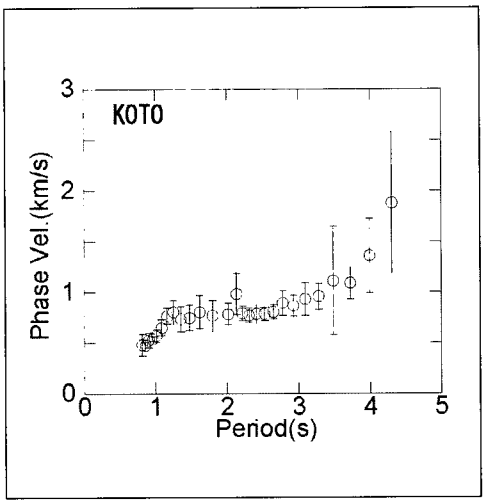


**Fig. 7. Rayleigh-wave phase velocity obtained from a microtremor array survey performed in downtown Tokyo by Yamanaka et al. (1995). Error bars indicate standard deviations.**

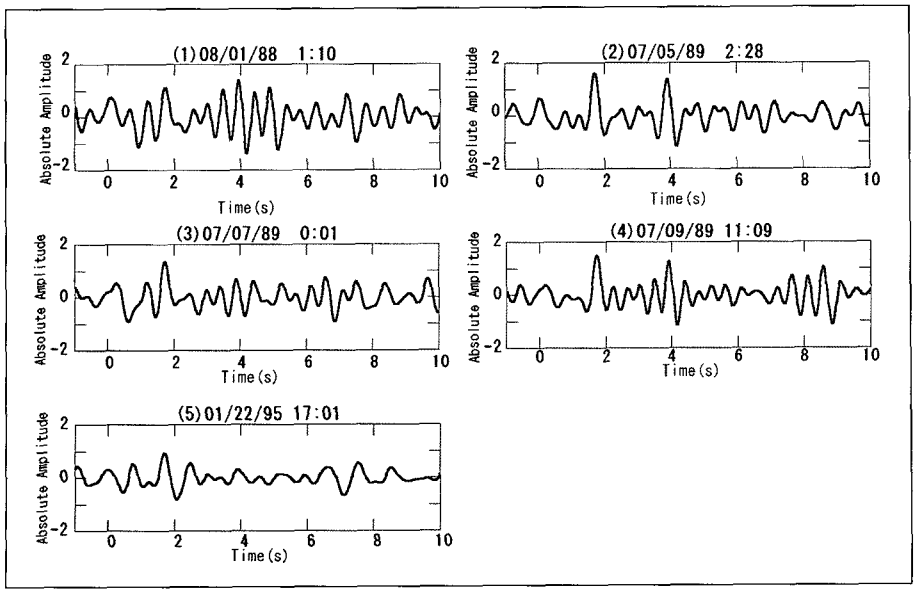


Fig. 8. Receiver functions calculated from earthquake records.

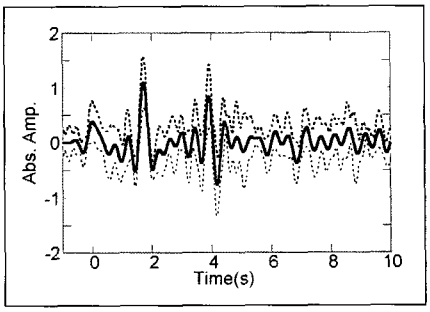


Fig. 9. Stacked receiver function. Broken line indicates standard deviation.

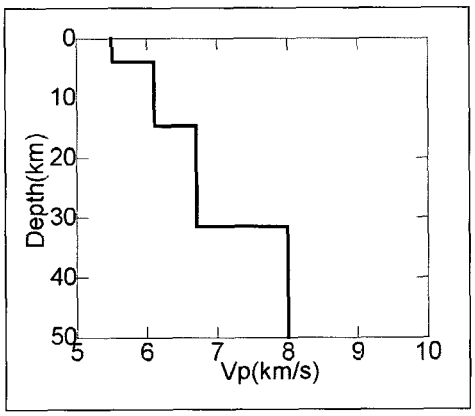


Fig. 10. P-wave velocity structure of the crust and mantle, used for calculation of incident angle at the top of basement of P waves from earthquakes used in calculation of observed receiver function.

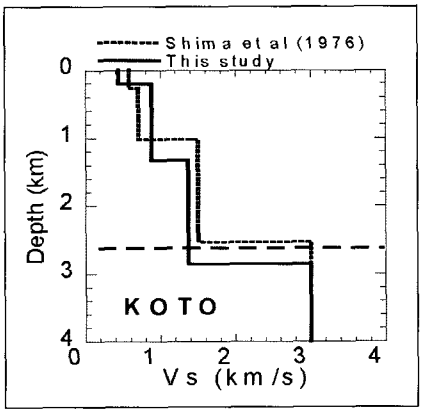


Fig. 11. Comparison between S-wave velocity structure obtained by joint inversion (solid line) and profile estimated from a seismic survey by Shima et al. (1976) (dotted line). The basement depth estimated by borehole investigation (Suzuki, 1999) is also shown by a broken line.

This model was modified from that used in epicentre determination by the Earthquake Research Institute of the University of Tokyo. The incident angles calculated for each event are different from each other and range from 35.3° to 34.0°. Therefore, the average incident angle, 34.6°, was used in the joint inversion. We again assumed a 4-layer model in the joint inversion, because there are three major geological units in the area. One is a Quaternary layer, and two units are of Tertiary age. The other parameters and assumptions were the same as we used in the preceding numerical experiments. The joint inversion was performed for the value of $p$ from 0.1 to 0.9 with an interval of 0.2, as in the case of numerical tests.

Figure 11 shows the model obtained by joint inversion with the value of $p = 0.5$, compared with the Vs-profile from S-wave travel time data in refraction surveys reported by Shima et al. (1976). The basement depth derived from a deep borehole near the site (Suzuki, 1999) is also shown in the figure. The S-wave velocities of each layer and the basement depth are in good agreement with each other. This suggests that the joint inversion can explore precisely deep structure despite the lack of enough long-period phase velocity information obtained by a microtremor array survey. Figures 12(a) and 12(b) show the comparisons between the observations of receiver function and phase velocity and the values

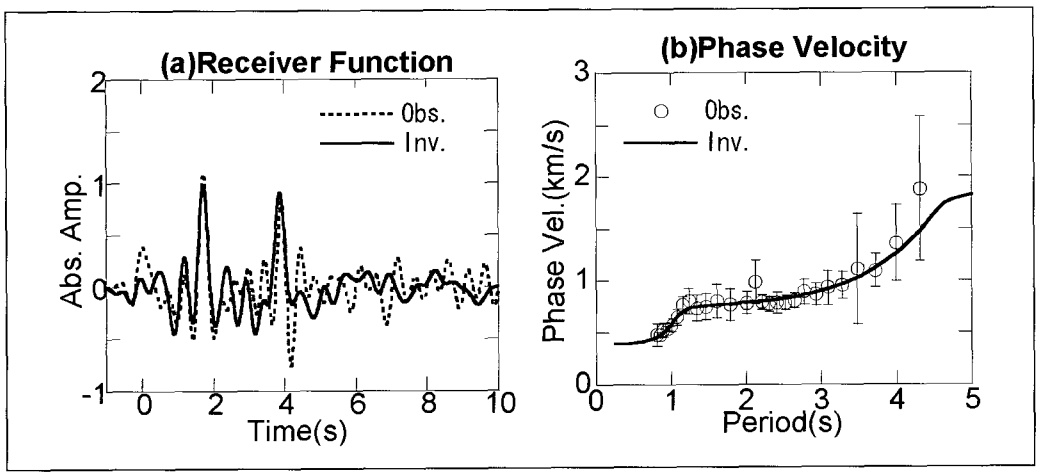


Fig. 12. Comparison of observations and synthetic data obtained from the S-wave velocity profile resulting from joint inversion. (a) Receiver function and (b) Rayleigh-wave phase velocity.

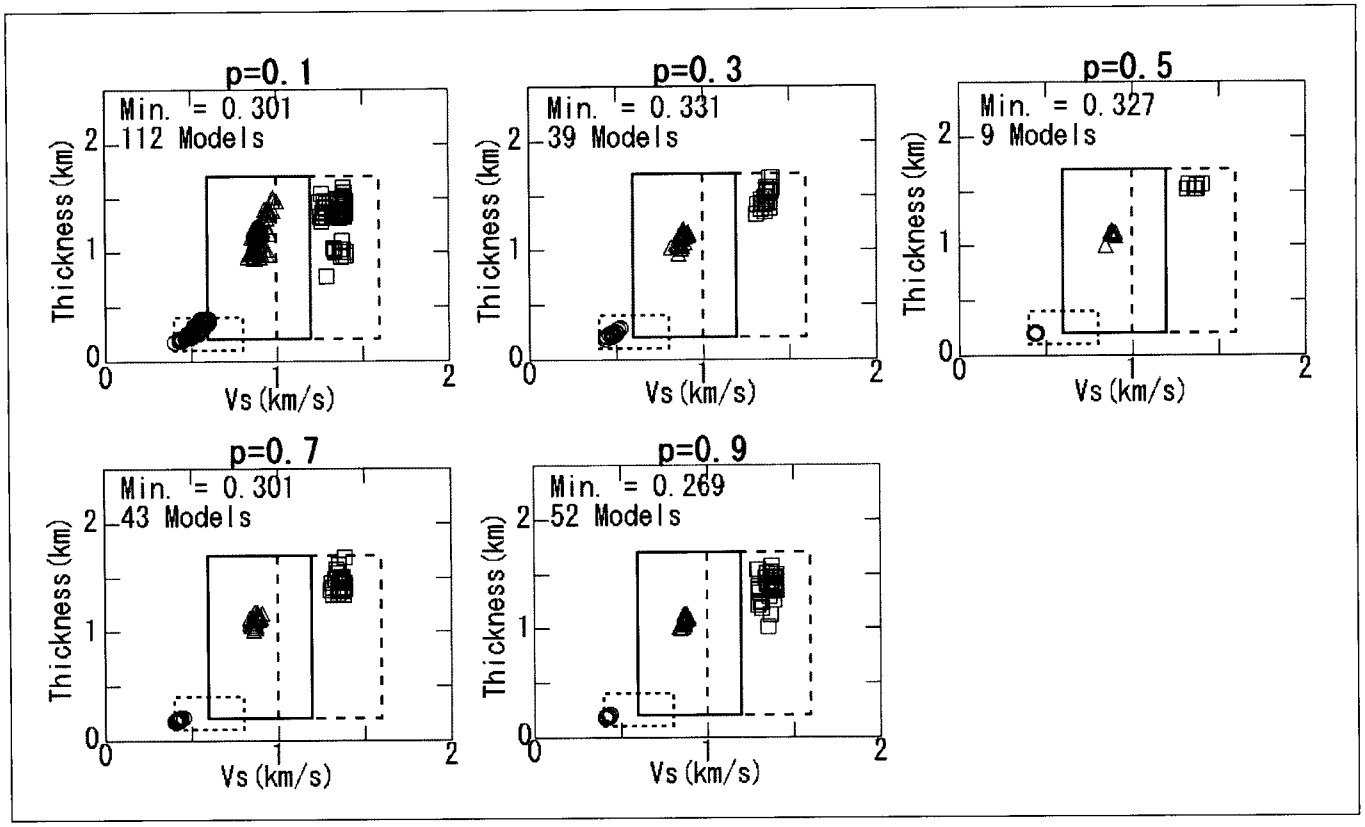


**Fig. 13. Parameter distributions of acceptable solutions from the joint inversion, for each value of $p$. The threshold was set to be the minimum misfit plus 0.05. Circles, triangles, and squares indicate the parameters of the first, second, and third layers, respectively. Rectangular areas shown by solid and broken lines indicate search limits for parameters of each layer.**

calculated from the final chosen model. The model can explain not only almost all of the major phases of the observed receiver function but also almost all of the observed phase velocity data. All of the inversion results for other values of $p$ showed trends similar to those shown here for the $p = 0.5$ case.

Parameter distributions for the acceptable solutions obtained from the joint inversion are shown in Figure 13 for each value of $p$. The misfit threshold for determining acceptable solutions was set to be equal to the value of the minimum misfit plus 0.05. The values of the minimum misfit and the numbers of the acceptable solutions are also shown in the figures. As in the numerical test case, the cases where there was less contribution from the phase velocity than from the receiver function (i.e., $p < 0.5$) shows that many acceptable solutions are distributed on a right-upward line, which suggests that the inversion was affected by trade-off between S-wave velocity and thickness in the receiver function. The cases with less contribution from the receiver function than from the phase velocity ($p > 0.5$) show that the parameters of the shallow part of the structure are distributed near one single point. However, the parameters describing the deeper parts of the structure are distributed over a larger area, indicating the lesser resolution of deep structure. In the case of $p = 0.5$, the parameters for all layers are distributed in the smallest areas, indicating that there are no local minima with a misfit nearly equal to the global minimum, and that the final model is unique and reliable.

Consequently, the joint inversion can provide models with less ambiguity and more reliability despite the lack of enough long-period phase velocity data provided by microtremor array surveys. The final model was in good agreement with the profiles obtained by previous studies, and could explain the observed receiver function and the phase velocity.

## DISCUSSION AND CONCLUSIONS

In this study, the method of joint inversion of receiver function and surface-wave phase velocity data, using genetic algorithms, was proposed to estimate a shear-wave velocity structure for deep sedimentary layers. Numerical experiments indicated that the proposed method could avoid the trade-off that arises when modelling receiver function data only. This method is also effective in reducing uncertainty in deep structure when modelling only surface-wave phase velocity data over a limited period range. Application of the method to observed data from Tokyo, Japan, resulted in good agreement with the profiles in previous studies. The case studies with various values of the influence parameter, $p$, indicated that the choice of $p = 0.5$ provides the highest reliability of the final model, which seems to show that receiver function and Rayleigh-wave phase velocity data equally constrain the shear-wave velocity structure.

In applying joint inversion method to actual data at a site without any information on subsurface structure in advance, a priori assumptions are important in successful determination of an S-wave velocity profile. For example, the number of layers is one of the critical parameters. Possibly, statistical criteria such as AIC, can be used to find an appropriate number of layers. Empirical relationships between velocities of P- and S-waves are also one of the important assumptions in this joint inversion. Although the contribution of P-wave velocity to the misfit of Rayleigh-wave phase velocity data is not significant, the effects of the choice of a different empirical relationship in joint inversion should be investigated before final determination of the S-wave profile at such a site.

## ACKNOWLEDGMENTS

The authors express their thanks to Yoshihiro Kinugasa and Kenichoro Kusunoki for valuable discussion and encouragement. The comments from the two reviewers and editors were helpful in improving the manuscript. Earthquake records used in this study were obtained by the Japan Meteorological Agency. This study is partly supported by a Grant-in-Aid for General Scientific Research (#14206081, #15510147) and Special Project for Earthquake Disaster Mitigation in Urban Areas from Japanese Ministry of Education, Culture, Sport, Science, and Technology.

## REFERENCES

Ammon, C.J., Randall G.R., and Zandt, G., 1990, On the nonuniqueness of receiver function inversion: *Journal of Geophysical Research*, **95**, 15303–15318.

Darbyshire, F.A., Priestley, K.F., White R.S., Stefansson, R., Gudmundsson G.B., and Jakobsdottir, S.S., 2000, Crustal structure of central and northern Iceland from analysis of teleseismic receiver functions: *Geophysical Journal International*, **143**, 163–184.

Haskell, N.A., 1960, The dispersion of surface waves in multilayered media: *Bulletin of the Seismological Society of America*, **50**, 657–679.

Haskell, N.A., 1962, Crustal reflection of plane P and SV waves: *Journal of Geophysical Research*, **67**, 4751–4767.

Horike, M., 1985, Inversion of phase velocity of long-period microtremors to the S wave velocity structure down to the basement in urbanized areas: *Journal of Physics of the Earth*, **33**, 59–96.

Julia, J., Ammon, C.J., Herrmann, R.B., and Correig, A.M., 2000, Joint inversion of receiver function and surface wave dispersion observations: *Geophysical Journal International*, **143**, 99–112.

Kagawa, T., Sawada, S., Iwasaki, Y., and Nanjo, A., 1998, S-wave velocity structure model of the Osaka sedimentary basin from microtremor array observations: *Journal of the Seismological Society of Japan (Zisin)*, **51**, 31–40.

Kitsunezaki, C., Goto, N., Kobayashi, Y., Ikawa, T., Horike, M., Saito, T., Kurota, T., Yamane, K., and Okuzumi, K., 1990, Estimation of P- and S- wave velocities in deep soil deposits for evaluating ground vibrations in earthquake: *Journal of the Japan Society for Natural Disaster Science*, **9**, 1–17.

Kobayashi, K., Uetake, T., Mashimo, M., and Kobayashi, H., 1998, An investigation on detection method of P to S converted waves for estimating deep underground structures: *Journal of Structural and Construction Engineering, Architectural Institute of Japan*, **505**, 45–52.

Koketsu, K., 1995, Underground structure in the Tokyo metropolitan area: *Geophysical Exploration (Butsuri-Tansa)*, **48**, 504–518.

Langston, C.A., 1979, Structure under Mount Rainier, Washington, inferred from teleseismic body waves: *Journal of Geophysical Research*, **84**, 4749–4762.

Last, R.J., Nyblade, A.A., Langston, C.A., and Owens, T.J., 1997, Crustal structure of the East African Plateau from receiver functions and Rayleigh wave phase velocities: *Journal of Geophysical Research*, **102**, 24469–24483.

Lomax, A., and Snieder, R., 1994, Finding of acceptable solutions with a genetic algorithm with application of surface wave group velocity dispersion in Europe: *Geophysical Research Letters*, **21**, 2617–2620.

Okada, H., 2003, *The microtremor survey method*: Society of Exploration Geophysicists.

Owens, T.J., Zandt, G., and Taylor, S.R., 1984, Seismic evidence for an ancient rift beneath the Cumberland Plateau, Tennessee: A detailed analysis of broadband teleseismic P waveforms: *Journal of Geophysical Research*, **89**, 7783–7795.

Priestley, K.F., Zandt, G., and Randall, G.E., 1988, Crustal structure in Eastern Kazakh, U.S.S.R.from teleseismic receiver function: *Geophysical Research Letters*, **15**, 613–616.

Sambridge, M., and Drijkoningen, G., 1992, Genetic algorithms in seismic waveform inversion: *Geophysical Journal International*, **109**, 323–342.

Sambridge, M., and Gallagher, K., 1993, Earthquake hypocenter location using genetic algorithms: *Bulletin of the Seismological Society of America*, **83**, 1467–1491.

Shibutani, T., Sambridge, M., and Kennett, B., 1996, Genetic algorithm inversion for receiver functions with application to crust and uppermost mantle structure beneath Eastern Australia: *Geophysical Research Letters*, **23**, 1829–1832.

Shima, E., Yanagisawa, M., Kudo, K., Seo, K., and Yamazaki, K., 1976, On the base rock of Tokyo 2, Observation of seismic waves generated from the 3rd Yumenoshima and Yoshikawa explosions: *Bulletin of the Earthquake Research Institute*, **51**, 45–61.

Suzuki, H., 1999, Deep geological structure and seismic activity in the Tokyo metropolitan area: *Journal of Geography*, **108**, 336–339.

Vozoff, K and Jupp, D.L.B., 1974, Joint inversion of geophysical data: *Geophysical Journal of the Royal Astronomical Society*, **42**, 977–991.

Yamanaka, H., Furuya, S., Nozawa, T., Sasaki T., and Takai, T., 1995, Array measurements of long-period microtremors in the Kanto Plain -Estimation of S-wave velocity structure at Koto-: *Journal of Structural and Construction Engineering, Architectural Institute of Japan*, **478**, 99–105.

Yamanaka, H., and Ishida, H., 1996, Application of genetic algorithms to an inversion of surface-wave dispersion data: *Bulletin of the Seismological Society of America*, **86**, 436–444.

Yamanaka, H., and Yamada, N., 2002, Estimation of 3D S-wave velocity model of deep sedimentary layers in Kanto plain, Japan, using microtremor array measurements: *Geophysical Exploration (Butsuri-Tansa)*, **55**, 53–65.

Zhao, L.-S., Sen, M.K., Stoffa, P.L., and Frohlich, C., 1996, Application of very fast simulated annealing to the determination of the crustal structure beneath Tibet: *Geophysical Journal International*, **125**, 355–370.

Zhou, R., Tajima, F., and Stoffa, P.L., 1995, Earthquake source parameter determination using genetic algorithm: *Geophysical Research Letters*, **22**, 517–520.

# 遺伝的アルゴリズムによる表面波位相速度とレシーバー関数の同時逆解析

黒瀬　健[1]・山中浩明[2]

**要　旨：**　この研究では、堆積層のS波速度構造を明らかにするために、遺伝的アルゴリズムの基づいた表面波の位相速度とレシーバー関数の同時逆解析方法を提案し、その適用性を検討している。S波速度3km/s程度の地震基盤までの深い堆積層を想定したモデルに対して基本モードのレイリー波の位相速度とレシーバー関数を計算し、ランダムノイズを与えたものを擬似的な観測データとして提案手法の数値実験を行った。その結果、同時逆解析によってS波速度と層厚の間のトレードオフの関係が改善されることがわかった。つぎに、関東平野中央部でのアレイ微動探査によるレイリー波の位相速度と地震観測記録から得られたレシーバー関数の同時逆解析を行い、深い地盤のS波速度構造を推定した。得られたモデルは、既存の探査結果とほぼ一致しており、提案手法の妥当性が確認された。

**キーワード：レシーバー関数、表面波、位相速度、アレイ微動探査、同時逆解析、堆積層、遺伝的アルゴリズム**

# 퇴적층들의 전단파 속도 평가를 위한 수신함수와 표면파 위상 속도의 통합 역산

Takeshi Kurose [1] and Hiroaki Yamanaka[1]

**요　약：**　이 연구에서는 유전자 알고리듬을 이용하여 수진기 함수와 표면파 위상 속도로부터 심부 퇴적층의 전단파 속도 구조를 결정하는 복합역산 방법을 제시하였다. 합성 탄성파 자료를 이용한 수치모형실험은 제시된 방법이 단지 수진기 함수만을 역산했을 때 발생하는 전단파 속도와 층 두께 사이의 trade-off 와, 표면파 위상 속도만을 역산했을 때 심부구조에서의 불확실성을 피할 수 있음을 보여주고 있다. 이 방법은 진앙거리 100 km 의 지진기록으로부터 얻은 수진기 함수들과 일본 Kanto 평원의 상시진동 배열 탐사로부터 얻은 레일리파의 위상속도에 적용되었으며, 추정된 심부구조는 선행된 굴절법 탐사 결과 및 심부 시추공 자료와 잘 일치하였다.

**주요어**：수진기 함수, 표면파, 위상속도, 상시진동 배열 탐사, 복합역산, 퇴적층, 유전자 알고리듬

1 東京工業大学　総合理工学研究科
（現、CRC ソリューションズ　地球科学部）
2 東京工業大学　総合理工学研究科

1 토쿄공업대학 종합이공학연구과